Electromagnetic Mechanism of Surface-enhanced Spectroscopy

George C. Schatz and Richard P. Van Duyne

Reproduced from:

Handbook of Vibrational Spectroscopy

John M. Chalmers and Peter R. Griffiths (Editors)

Electromagnetic Mechanism of Surface-enhanced Spectroscopy

George C. Schatz and Richard P. Van Duyne
Northwestern University, Evanston, IL, USA

1 INTRODUCTION

The purpose of this article is to review the electromagnetic mechanism (EM) of surface-enhanced spectroscopy (SES). This mechanism has played an important role in our understanding of SES since the original papers on surface-enhanced Raman spectroscopy (SERS),[1–3] and in many respects it is a mature topic, having been the subject of numerous reviews.[4–13] However, there are many features of the comparison with experiment that are still rather vague, and this has served as a source of confusion in assessing the role of other mechanisms, such as chemical mechanisms, in SES.[14] Since it has now been several years since the topic has been discussed in a general way, it seems appropriate to present a new review in which the current status of the EM is considered. Much of this discussion will center on SERS, as it is still the most extensively studied of the enhanced surface spectroscopies, but other spectroscopic methods will also be brought in where relevant, as the comparison of theory and experiment for other methods has in many cases provided important new insights into the predictive ability of the theory. The other methods that will be considered include surface-enhanced second harmonic generation (SESHG) and surface-enhanced hyper-Raman spectroscopy (SEHRS). We will also discuss recent advances in the electromagnetic description of linear extinction and scattering that are relevant to SES. Much of the discussion will focus on isolated nanoparticles, as this provides the simplest problem that still exhibits all the features of SES that are also found in more complex systems.

Let us begin by defining what we mean by the EM. When an electromagnetic wave interacts with any metal surface, be it smooth or rough, the field near the surface is different from that far away from it. If the surface is flat, the application of Maxwell's equations to determine the field near the surface, and the dependence of Raman intensities on the incident and scattered angles, was worked out by Greenler and Schlager well before the discovery of SERS.[15] There is a small enhancement in Raman intensity compared with that in the absence of the surface, on the order of a factor of 10 or less for metals like Ag, arising primarily from coherent superposition of the incident and reflected fields at the position of the molecule doing the scattering. Note that although collective excitations of the conduction electrons known as surface plasmons exist for Ag at frequencies of roughly $\hbar\omega = 3.5$ eV, they cannot be excited by the electromagnetic field when irradiating a flat surface, as momentum cannot be conserved in the excitation process.

If the surface under consideration is roughened, then the electrodynamics of the irradiated surface become much more interesting. The key result is that surface plasmons can now be excited by electromagnetic radiation, resulting in enhanced electromagnetic fields close to the surface.[16,17] In Raman scattering, the intensity depends on the square of the incident field strength, and as a result, the intensity is enhanced relative to what it would be in the absence of the surface. The Raman emitted field may also be enhanced, though generally by a different amount than the incident field, since the frequency is different. Also the field is spatially different as it arises from an oscillating dipole located at the position of the emitting molecule. The overall enhancement associated with the incident and emitted fields is what we shall consider to be the EM contribution to SERS. An attractive feature of this mechanism

is that the enhancement and its wavelength dependence may be estimated using calculations that require only the size and shape of the metal particles or surface involved, and the relevant dielectric constants. A number of calculations of the enhancement based on this idea have appeared in the literature, including work by Kerker and co-workers,[18–21] Gersten and Nitzan,[22] Adrian,[23] Metiu,[11] Barber and co-workers,[24] Schatz and co-workers[25,26] and Kottmann and co-workers[27] on isolated particles. In addition, several groups have modeled SERS on gratings,[28–30] Laor and Schatz[31,32] considered assemblies of particles on surfaces, and Sanchez-Gil and Garcia-Ramos[33] and others (cited in Sanchez-Gil and Garcia-Ramos[33]) have studied randomly roughened surfaces. The theory predicts large enhancements for all of these structures provided that the metal involved has narrow plasmon resonances at convenient frequencies for Raman measurements (i.e. in the visible region of the spectrum). In the next section, we examine what this means for a variety of different materials, and we also consider what the model predicts for wavelengths that have not been considered in traditional experiments, but which are now becoming accessible thanks to advances in laser and detector technology.

To clarify the qualitative definition of the EM just given, we begin the next section with a simple quasistatic model of the EM enhancement. In this model, we consider that molecules are adsorbed on the surface of a sphere that is small compared with the wavelength of light, so that Maxwell's equations may be replaced by the LaPlace equation of electrostatics. The frequency dependent dielectric constant is still used in this calculation. This model contains most of the essential issues that are important to SES, even for SES on roughened electrode surfaces, but it is not useful for quantitative estimates of enhancements, as the plasmon resonances associated with spherical particles lie far enough to the blue that even for the noble metals they are damped by interband transitions and other excitations, i.e. the metals are absorbers at the plasmon frequencies. More quantitative estimates of enhancement factors are obtained from models that allow the metal particles to have spheroidal shapes. We discuss such particles in the next section, although to keep the mathematics simple, we omit most details, and emphasize instead the results of calculations and comparisons with experiment. However, even these calculations are not quantitative unless a number of additional issues are addressed. For example, the correct treatment involves electrodynamics not electrostatics, and often the differences are significant even when the particles are only 10% of the wavelength of light in longest dimension. Approaches for treating this issue range from brute force numerical solutions of Maxwell's equations[24,26,27] to perturbation corrections of the electrostatic treatment.[25] Another problem arises in the values of the metal particle dielectric constants. Usually these are taken from measurements on bulk metals, but for small particles (smaller than the conduction electron mean free path) this choice is inappropriate, and corrections are necessary.[34]

Extensions and additional complications in applications of the EM to single-metal particles are the subject of later sections of this review. One issue is the influence of the adsorbate on the interaction of the electromagnetic field with the metal particles or surfaces. (Usually the adsorbate has been neglected in the spheroid calculations noted above.) This is especially important when the adsorbates absorb light at the incident or scattered frequencies, i.e. resonant Raman scattering, as then the plasmons can be damped by interaction with the adsorbate,[35,36] but it also plays a role in nonresonant scattering,[37] when it contributes to the coverage dependence of the Raman intensities.

Another important extension to the EM that we discuss later arises in the consideration of nonlinear surface spectroscopies, including SESHG and SEHRS. As long as the nonlinear polarization arises from the electromagnetic field gradient near the particle surface (the jury is still out on this[38–41]), it is straightforward to extend the electromagnetic model to the description of nonlinear surface optical spectroscopy by factoring in the additional powers of the incident field at the appropriate wavelength. This model implicitly assumes that SESHG is actually incoherent hyper-Rayleigh scattering, which for isolated nanoparticle systems is probably a reasonable assumption. Comparisons with experiment can then be made, and these provide two important pieces of information concerning the enhancement that are not available from SERS alone. First, the enhancement can be measured for materials and wavelengths that are not generally accessible to SERS. This is especially true for SESHG, where even materials like Pt have been studied.[42] Second, the comparison of electromagnetic model enhancements with experimental enhancements provides an independent determination of the relative magnitudes of the electromagnetic and nonelectromagnetic contributions to SERS. In addition, one can use the comparison of SERS and SEHRS to study the local symmetry experienced by the adsorbed molecules, as the selection rules for SERS and SEHRS are quite different.

Another useful application of electromagnetic theory that we consider in this review is to the calculation of extinction and scattering cross-sections for the same nanoparticles as are considered in calculating SERS spectra. These cross-sections may be obtained from the same solutions of Maxwell's equations as are used to model SERS, but they depend on the asymptotic properties of the solutions rather than surface fields. For very small spherical particles, there is a close relationship between these cross-sections

and the SERS excitation profiles (which will be given in the next section), so that both have plasmon peaks at the same wavelength. However, for nonspherical particles and larger spherical particles there are significant differences in wavelength dependence that provide important information about the EM. In addition, we can learn much from extinction spectra about the influence of solvent and substrate dielectric properties on EM enhancements.

In the last section of this review, we consider applications of the EM to models of the surface other than a single-metal particle. Such models can take many different forms, ranging from a small number of interacting spheres or other shapes, to large assemblies of particles, either randomly arranged or in regular arrays, and to gratings.

While the discussion to this point has emphasized how the EM has been developed and extended, it is also important to consider how the EM fits into the larger picture that theorists have attempted to develop of the complete enhancement process. A common definition is to assume that any part of the surface enhancement that is not accounted for using the EM involves the "chemical mechanism". With this definition, "chemical mechanisms" refer both to enhancements that arise from interactions between molecule and surface that require orbital overlap between the molecule and metal wavefunctions, and to those interactions that do not require overlap. The most commonly considered interaction that requires overlap occurs when charge transfer between surface and adsorbate leads to the formation of excited states that serve as resonant intermediates in Raman scattering.[43] Interactions that do not require overlap arise from electromagnetic coupling between the vibrating molecule and the metal. These interactions can occur either at the vibrational frequency or at optical frequencies. The former case involves interaction of the oscillating dipole and/or quadrupole field of the vibrating adsorbed molecule with the surface electrons. Such fields would be expected to modulate the metal surface dielectric properties (especially at frequencies close to the surface plasmon frequency where the metal is highly polarizable), leading to Raman shifted reflection of light from the surface. This mechanism is sometimes called the Raman reflectance mechanism,[44–48] and it can also arise from modulated overlap between the molecule and surface orbitals.[47,48] The electrostatic part of Raman reflectance has been explored by Dignam and co-workers,[49] who use the term surface phonon-induced Raman scattering (SPIRS) to describe this mechanism. This mechanism is most important for small metal particles (25 Å), where it can be comparable in enhancement to the EM. However, its importance drops off rapidly with particle size. It is unfortunately not clear how important this mechanism is for conditions that model real experiments.

Electromagnetic coupling between the adsorbate and surface at optical frequencies arises from the dipole moment in the adsorbed molecule that is induced by the applied electromagnetic field. This dipole will polarize the metal electrons at optical frequencies, leading to a change in the effective polarizability of the adsorbate. This mechanism, which is just another part of the polarization response of the adsorbate/substrate system that also produces the EM,[22] is often called the image field mechanism,[10] as it can be pictured as arising from interaction of the molecule with its image in the metal. However, the magnitude of the enhancement arising from this effect is significant only when the molecule is too close to the surface to model its interaction accurately using electrodynamic theory with point dipoles, so in most treatments of the EM[22] it has ben explicitly excluded from consideration. This is not correct, of course, but the treatment of molecules close enough to the surface to experience orbital overlap is best done using approaches that consistently combine the electronic wavefunctions of the molecule and metal in describing the electrodynamic response of the system. So far, there have been relatively few calculations of this type,[45,50–52] and all have made severe enough approximations that it is hard to quantify the true significance of the image effect. Most of the SERS enhancement can be explained using electrodynamics models that ignore the image effect, so it seems best to ignore it.

2 ELECTROMAGNETIC MECHANISM OF SURFACE-ENHANCED RAMAN SPECTROSCOPY FOR ISOLATED METAL PARTICLES

2.1 A simple model: quasistatic treatment of an isolated sphere

The model that we will develop consists of a single metal sphere, small compared to the wavelength of light, which is irradiated by a laser field. Raman scattering arises from molecules that are adsorbed on the surface of this sphere. For now we will ignore the molecules in determining the field near the surface, and assume that the sphere is embedded in a medium (which could be vacuum or solvent) of dielectric constant ε_o. The dielectric constant inside the metal sphere is denoted by ε_i, and for now we take this dielectric constant to be independent of the size of the sphere.

We take the electric field of the incident electromagnetic wave to be $\mathbf{E}_o$, a vector that points along the z-axis, and that can be assumed independent of coordinates for distances at least as large as the sphere. Under these conditions, Maxwell's equations may be approximated by LaPlace's equations to determine the field both inside and outside the

sphere. The resulting field outside the sphere, $\mathbf{E}_{\text{out}}$, can then be written as:

$$\mathbf{E}_{\text{out}} = E_{\text{o}}\mathbf{z} - \alpha E_{\text{o}}\left[\frac{\mathbf{z}}{r^3} - \frac{3z}{r^5}(z\mathbf{z} + x\mathbf{x} + y\mathbf{y})\right] \tag{1}$$

where the first term is the applied field, and the second is the induced dipole that results from polarization of the sphere electron density. α is the metal polarizability, x, y, z, r, $\mathbf{x}$, $\mathbf{y}$, $\mathbf{z}$ are the usual Cartesian coordinates, radial distance and Cartesian unit vectors, respectively and E_{o} is the magnitude of $\mathbf{E}_{\text{o}}$. For a metal sphere with the dielectric constants indicated above, the polarizability is

$$\alpha = ga^3 \tag{2}$$

where a is the sphere radius and

$$g = \frac{\varepsilon_{\text{i}} - \varepsilon_{\text{o}}}{\varepsilon_{\text{i}} + 2\varepsilon_{\text{o}}} \tag{3}$$

Note that the polarizability is a number that is on the order of the sphere volume in the limit of zero frequency, as in that case ε_{i} is $-\infty$. However, whenever the real part of ε_{i} equals $-2\varepsilon_{\text{o}}$ and the imaginary part is small, α becomes very large, and as a result the induced field becomes large. It is this induced field that is responsible for the electromagnetic enhancement. Note that this plasmon resonance condition requires the real part of ε_{i} to be large in magnitude and negative, and this is always the case for a free electron metal at long enough wavelengths. In addition, the formula says that the plasmon resonance wavelength will change when the dielectric constant ε_{o} of the external medium is varied. Indeed, since the metal dielectric constant typically increases (becomes less negative) as wavelength decreases, the resonance condition will be satisfied for longer wavelengths, i.e. red-shifts, as solvent dielectric constant increases.

The Raman intensity depends on the absolute square of $\mathbf{E}_{\text{out}}$ which we denote as E^2_{out}, evaluated at the surface of the sphere (i.e. $r = a$). From equation (1), this is given by

$$E^2_{\text{out}} = E^2_{\text{o}}[|1 - g|^2 + 3\cos^2\theta(2\,\text{Re}(g) + |g|^2)] \tag{4}$$

where θ is the angle between the applied field direction and the vector $\mathbf{r}$ that locates positions on the sphere surface. Note that if $|g|$ is large, equation (4) reduces to $E^2_{\text{out}} = E^2_{\text{o}}|g|^2(1 + 3\cos^2\theta)$. This indicates that the largest field intensities are obtained for angles θ equal to zero or 180°, i.e. along the polarization direction. Also, the ratio of the largest to smallest field enhancement as a function of θ is 4, and the angle integrated expression is 1/2 the peak intensity.

In Raman scattering the applied field induces an oscillating dipole in the adsorbed molecule. This dipole then radiates, and the component of this radiation that has been shifted by the vibrational frequencies of the molecule determines the Raman scattering intensity. In SERS the field in equation (4) determines the magnitude of the induced dipole, but there is also the possibility of enhanced emission from this dipole. This enhancement is more difficult to evaluate, as unlike the applied field E_{o} which is accurately described as being constant over the volume of the sphere, the emitted field is more complex. The proper treatment of this field has been given by Kerker *et al.*[19,20] To a first approximation that is appropriate for small particles (see Kerker[21]), the enhancement is determined by an expression similar to equation (4), but evaluated at the Raman-shifted frequency. If we consider molecules located at the position of maximum enhancement and consider only the limit $|g| \gg 1$, then the overall enhancement arising from incident and scattered fields is approximately

$$\mathscr{E}_{\text{R}} = \frac{E^2_{\text{out}}E'^2_{\text{out}}}{E^4_{\text{o}}} = 16|g|^2|g'|^2 \tag{5}$$

where the primed symbols refer to fields evaluated at the scattered frequency. The corresponding angle averaged enhancement factor would be smaller than this by a factor of 4. Equation (5) is identical to one derived by Kerker *et al.*[19,20] using more rigorous theory. For small Stokes shifts, $|g|$ and $|g'|$ maximize at approximately the same wavelength, in which case if $|g|$ and $|g'|$ are both approximately 10 in magnitude, then the enhancement will be approximately 10^5. If we use the free-electron Drude model for the metal dielectric constant:

$$\varepsilon_{\text{i}} = 1 - \frac{\omega^2_{\text{p}}}{\omega(\omega + \text{i}\gamma)} \tag{6}$$

where ω_{p} is the plasmon frequency and γ is the plasmon width, then the peak magnitude of g will be roughly 10 when the ratio of the plasmon frequency to plasmon width is roughly 10. There are several materials such as Ag where the peak $|g| \geq 10$. However the free electron model for the dielectric constant is rarely sufficiently accurate for this prediction to be quantitative. In fact, electromagnetic enhancements are generally rather small for spherical particles because the surface plasmons for most materials are far enough to the blue that γ is large (typically due to interband transitions). Larger enhancements arise for prolate spheroidal objects, as the plasmon resonances for such objects occur at frequencies that are red-shifted relative to spherical particles to frequencies where the plasmon width is sufficiently small to make $|g|$ 10 or larger. For this reason we turn our attention in the next section to the electrodynamics of spheroidal particles.

The results obtained to this point are related closely to the extinction and scattering cross-sections for spherical particles, as obtained from the long wavelength limit ($a/\lambda \ll 1$) of Mie theory.[53] In particular, if we define $x = 2\pi a(\varepsilon_{\text{o}})^{1/2}/\lambda$, then the extinction cross-section Q_{ext} is:

$$Q_{\text{ext}} = 4x\ \text{Im}(g) \tag{7a}$$

and the scattering cross-section Q_{sca} is:

$$Q_{\text{sca}} = \frac{8}{3}x^4|g|^2 \tag{7b}$$

where g is still given by equation (3). Evidently, if we leave out the x^4 prefactor (which varies as λ^{-4}), the wavelength dependence of equation (7b) is the same as the large $|g|$ limit of equation (4). In addition, as long as the plasmon width is much smaller than the plasmon energy, the extinction cross-section has the same wavelength dependence (after leaving out the x factor) as the large $|g|$ limit of equation (4). Since the extinction cross-section is much larger than the scattering cross-section for a small metal particle, it is extinction that is most often compared to SERS excitation profiles. What we see therefore is that in the small particle limit, SERS excitation and extinction plasmon peaks and widths should be the same.

2.2 Electrostatics of isolated spheroids

The exact analytical solution to the electrodynamics of spheroidal particles is very complex, so the work done has involved either numerical solutions of Maxwell's equations[24,26] or analytical electrostatic solutions[19,20,23,25] that are valid only for small particles. Although the numerical solutions are more accurate, the electrostatic solutions are more instructive. Fortunately, for particle sizes of significant interest to the experiments (<100 nm), the two theories give very similar results.

If we consider a spheroid whose major axis is of length $2b$ and minor axis $2a$, with a constant field E_{o} applied along the major axis, then an explicit expression for the Raman enhancement factor for molecules that are randomly distributed on the spheroid surface (i.e. averaged over the surface) has been given by Zeman and Schatz[25] as follows:

$$\mathscr{E}_{\text{R}} = R(\omega)R(\omega - \Delta) \tag{8}$$

where

$$R(\omega) = |1-g|^2 + \left[\frac{2\,\text{Re}(1-g)g^*}{Q_1(\xi_{\text{o}})} + \frac{|g|^2}{Q_1^2(\xi_{\text{o}})(\xi_{\text{o}}^2-1)}\right] \times \left[\frac{-(\xi_{\text{o}}^2-1)^{1/2} + \xi_{\text{o}}^2\sin^{-1}(1/\xi_{\text{o}})}{(\xi_{\text{o}}^2-1)^{1/2} + \xi_{\text{o}}^2\sin^{-1}(1/\xi_{\text{o}})}\right] \tag{9}$$

$$\xi_{\text{o}} = \left(1 - \frac{a^2}{b^2}\right)^{-1/2} \tag{10}$$

$$Q_1(\xi_{\text{o}}) = \frac{1}{2}\xi_{\text{o}}\ln\left(\frac{\xi_{\text{o}}+1}{\xi_{\text{o}}-1}\right) - 1 \tag{11}$$

and

$$g = \frac{\varepsilon_{\text{i}} - \varepsilon_{\text{o}}}{\varepsilon_i + \chi\varepsilon_{\text{o}}} \tag{12}$$

The parameter χ in equation (12) is given by

$$\chi = -1 + \frac{1}{(\xi_{\text{o}}^2-1)\left[\frac{\xi_{\text{o}}}{2}\ln\left(\frac{\xi_{\text{o}}+1}{\xi_{\text{o}}-1}\right) - 1\right]} \tag{13}$$

Note that g in equation (12) is a generalization of that in equation (3). In fact the parameter χ equals 2 for a sphere, but for prolate spheroids, i.e. those with $b > a(\xi_{\text{o}} > 1)$, χ is larger than 2 and for oblate spheroids ($\xi_{\text{o}} < 1$) it is less than 2. When χ is greater than 2, the plasmon resonance condition, $\text{Re}(\varepsilon_{\text{i}} + \chi\varepsilon_{\text{o}}) = 0$, is satisfied for a wavelength that is to the red of that for a sphere (due to the fact that for metals, the real part of ε_{i} is, according to equation (7), more negative for longer wavelengths). Of course this also means that for oblate spheroids, the resonance will be blue-shifted relative to a sphere. However, it should be noted that the resonance described here refers to an incident field with the electric polarization parallel to the symmetry axis of the spheroid. There is another plasmon resonance associated with excitation perpendicular to the symmetry axis. This resonance is identical in frequency to the parallel resonance for a sphere, but it shifts in the opposite direction for a spheroid, i.e. blue-shifting for prolate spheroids and red-shifting for oblate spheroids. Indeed, the expression for g in equation (12) still applies, but the expression for χ is:

$$\chi = -1 - \frac{1}{\left[\frac{1}{2}\xi_{\text{o}}(\xi_{\text{o}}^2-1)\ln\left(\frac{\xi_{\text{o}}+1}{\xi_{\text{o}}-1}\right) - \xi_{\text{o}}^2\right]} \tag{14}$$

Thus we see that both oblate and prolate spheroids have plasmons that are red-shifted relative to the sphere case. Since most SERS-active metals (Ag, Au, Cu) exhibit free electron-like behavior at long wavelengths, it is the red-shifted plasmon resonance that contributes most to SERS. Thus nonspherical particles, either prolate or oblate, give larger SERS intensities than spheres. In addition, we see that increasing the dielectric constant of the external medium, ε_{o}, leads to additional red-shifting of the plasmon resonances, just as with the sphere case that we described earlier.

Equation (9) refers to the enhancement averaged over the surface of the spheroid. In some applications it is also of interest to have an expression for the enhancement as a function of location on the surface. This expression is given by:

$$R(\omega,\eta) = |1-g|^2 + \left[\frac{2\,\text{Re}[(1-g)g^*]\eta^2}{Q_1(\xi_{\text{o}})(\xi_{\text{o}}^2-\eta^2)} + \frac{|g|^2\eta^2}{Q_1^2(\xi_{\text{o}})(\xi_{\text{o}}^2-1)(\xi_{\text{o}}^2-\eta^2)}\right] \tag{15}$$

Note that this expression depends on the spheroidal coordinate η, which is related to the usual spherical polar coordinate θ via:

$$\eta = \cos\theta \sqrt{\frac{\xi_o^2 - 1}{\xi_o^2 - \cos^2\theta}} \tag{16}$$

Some specific examples of results based on equations (8–16) will be given later. First, however, we need to discuss corrections and improvements to them, as these equations are not yet sufficiently accurate to be useful.

2.3 Improvements to the spheroid model

The treatment up to this point has considered an isolated spheroid with dielectric constant ε_i interacting with an electromagnetic field that is treated in the static limit. It turns out that for particle sizes of most relevance to the experiments (5–200 nm) and excitation wavelengths in the range 400–1000 nm, there are two corrections to this development that need to be implemented in order to obtain realistic results. These are electrodynamics corrections, which in lowest order are called radiation damping and dynamic depolarization, and corrections to the dielectric constant of the particle that are important when the particle is smaller than the conduction electron mean free path.

2.3.1 Electrodynamic corrections

If one solves Maxwell's equations exactly for a spheroid, and then expands the solution in powers of the photon wavenumber $k(k = \omega/c)$, one finds corrections to the static $(k = 0)$ limit that can be thought of as coming from two sources. One is radiation damping, which refers to reduction in the polarization induced by the applied field that results from emission of radiation by the induced dipole (i.e. the dipole emits so fast that its size is diminished). The second is dynamic depolarization, which refers to interference between radiation emitted at different points on the surface of the particle. A simple argument for including these effects has been given by Meier and Wokaun.[54] Their theory is developed specifically for spheres, but it can be extended approximately to spheroids[55] through the following argument.

When a particle is irradiated by an external field, the induced dipole μ_{ind} in the spheroid is given in the static limit by

$$\mu_{ind} = \alpha_o E \tag{17}$$

where the spheroid polarizability α_o is given by

$$\alpha_o = \frac{1}{3}\frac{g\xi_o f^3}{Q_1(\xi_o)} \tag{18}$$

and

$$f = (b^2 - a^2)^{1/2} \tag{19}$$

Here E is the (enhanced) applied field. Inclusion of electrodynamics corrections leads to the modified expression

$$\mu_{ind} = \alpha_o(E + E_{rad}) \tag{20}$$

where

$$E_{rad} = \left(\frac{k^2}{b} + \frac{2i}{3}k^3\right)\mu_{ind} \tag{21}$$

and the wavenumber k was defined previously. The term in E_{rad} proportional to k^2 describes dynamic depolarization, while that proportional to k^3 describes radiative damping. Substitution of equation (21) into equation (20) leads to a modified expression for the induced dipole moment

$$\mu_{ind} = \left(1 - \frac{\alpha_o k^2}{b} - \frac{2ik^3\alpha_o}{3}\right)^{-1}\alpha_o E \tag{22}$$

Note that the second and third terms in the denominator in equation (22) are proportional to the particle polarizability α_o. In the $k \to 0$ $(\lambda \to \infty)$ limit where $g \to 1$, α_o is roughly the particle volume (proportional to f^3 in equation 18) so these two terms are proportional to particle volume (or area for the first term) divided by λ^3 (λ^2 for the first term) and hence are negligible. However, at the plasmon resonance frequency, $|g| \gg 1$, so these terms can be significant ($k^3\alpha_o \approx 1$) even when the particle size is only 10% of the wavelength λ. In addition, it should be noted that the effect of these terms is both to reduce μ_{ind} and to shift where it peaks to longer wavelengths. Of course it is important to realize that equation (22) is correct only through the k^3 term in an expansion of the exact solution of Maxwell's equations in powers of k, so errors are likely whenever $k^3\alpha_o$ is of order unity. In that case one should use more accurate approaches.[24,26,27]

To incorporate the electrodynamic corrections into the field enhancement factor $R(\omega)$, we have multiplied equation (9) by the absolute square of the term in parentheses in equation (22).

2.3.2 Size-dependent dielectric constants

It is known that the dielectric constant of a metal particle becomes size dependent whenever the particle is smaller than the conduction electron mean-free path. For noble and alkali metals, this applies to particles that are roughly 20 nm or less in smallest dimension. A number of models for this effect have been given, ranging from classical models[56,57] that determine the rate of scattering of the conduction electrons from the particle surface, to quantum models[34,58–60] in which the dielectric constant of the particle is calculated using an approximate electronic structure theory (free electron in a cavity[34,46,48] or jellium[61]). The results of these

studies show that the most significant influence of particle size as long as the particles are not too small is in broadening of the plasmon width. Other features such as blue- (for alkalis) or red- (for silver) shifting of the resonance frequency and the appearance of multiple absorption bands have been found in the context of gas-phase metal cluster spectroscopy[61] but have been less prominent in SES studies.

To describe the plasmon width broadening associated with small particles, it is convenient to consider the Drude model dielectric constant (equation 6). The width γ can be considered to be composed of two contributions, a bulk width γ_b and a (size-dependent) surface contribution γ_S such that

$$\gamma = \gamma_b + \gamma_S \tag{23}$$

For a spherical particle, classical models show that γ_S is inversely proportional to particle radius, so we write

$$\gamma_S = A\frac{v_F}{R} \tag{24}$$

where v_F is the Fermi velocity (v_F/R being the classical rate of scattering from the particle surface) and A is a dimensionless constant that equals unity according to classical theory. The latest jellium estimate of A is 0.7636 but earlier theories based on free-electron models suggested that $A = 1.16$.[34] Fortunately, the value of A is close enough to unity in both these expressions that the classical expression can be used without serious error for typical SERS experiments. The classical models have also been used to obtain formulas like equation (24) for other particle shapes. In this case, one sets A to unity, and replaces R by an effective particle length L_{eff}. For a spheroid, L_{eff} is given by[60]

$$L_{\text{eff}} = \frac{4}{3}b\left[\left(\frac{\xi_o^2+1}{\xi_o^2-1}\right)^{1/2} - \sin^{-1}\left(\frac{1}{\xi_o}\right) + (\xi_o^2-1)^{3/2}\times\ln\left(1-\frac{1}{\xi_o^2}\right)\right]\times\left[\xi_o^2(\xi_o^2-1)^{-1}\sin^{-1}\left(\frac{1}{\xi_o}\right) + \frac{1}{(\xi_o^2-1)^{1/2}}\right]^{-1} \tag{25}$$

Note that this expression reduces to $L_{\text{eff}} = b$ for $b = a$ (a sphere), and to $L_{\text{eff}} = 16a/3\pi$ for $b \gg a$ (a needle).

The main consequence of the increase in plasmon width associated with decreased particle size is suppression of the field enhancement *without* changing its frequency or shape dependence. Of course the theory presented here is not appropriate for *very* small particles (<2 nm), so caution should be used in applications.

2.4 Current status of theory/experiment comparisons

Let us begin this section by showing some representative SERS enhancement factors from the electromagnetic model. The results to be presented were calculated for spheroids using equations (8) and (9) with the electrodynamic corrections from equation (22) and using dielectric constants that incorporate the size-dependent plasmon width based on equations (23) and (24). Except for the size-dependent dielectric constants, the Raman enhancements obtained from this procedure are nearly identical to those from the accurate electrodynamic calculations of Barber *et al.*[24] and Yang *et al.*[26] (Barber *et al.* and Yang *et al.* assume that dielectric constants are size independent.) The dielectric constants used in these calculations are either from Palik[62] or from Hagemann *et al.*[63] The former are more recent, and probably more accurate, but the latter were used extensively in earlier work.[11,25,55,64] In a few cases, we give comparisons between the results to indicate the magnitude of the differences. Figure 1 shows the field enhancement R and Raman enhancement $\mathscr{E}_R$ as a function of wavelength for silver spheroids of varying b/a between 1 : 1 and 5 : 1. The semimajor axis b has in all cases been fixed at $b = 25$ nm, and the Stokes shift $\Delta\omega$ is 1500 cm^{-1}. Here we have used dielectric constants from Palik, but equivalent results from the Hagemann dielectric constants are given in Zeman and Schatz.[25] The surrounding dielectric constant ε_o has been taken to be unity.

Figure 1 shows typical plasmon excitation profiles, with the plasmon frequency shifting to the red as the spheroid becomes more prolate. The Raman enhancements are large, as large as 10^5, and they are largest for spheroids having a plasmon wavelength of about 600 nm. These Raman enhancements are a factor of about 10 smaller than are obtained if the corrections of the previous section are not used. These corrections have been left out in some of the past work,[18–20,22,27] but it is likely that the results in Figure 1 are more realistic for typical SERS measurements.

In some past calculations, only the field at the tip of the spheroid has been used in calculating enhancements. Again this is probably not representative of typical SERS measurements. However, recent single-molecule SERS measurements[65–69] have generated significant interest in what is the largest EM enhancement near the surface of particles with tips. A variety of estimates are available[18–20,22,27,70] with the largest EM SERS enhancements being around 10^{10}. Figure 2 shows how the Raman enhancement varies with polar angle θ as one goes around the spheroid. The figure includes results for all five spheroids from Figure 1, with the wavelength chosen to be close to the plasmon peak for

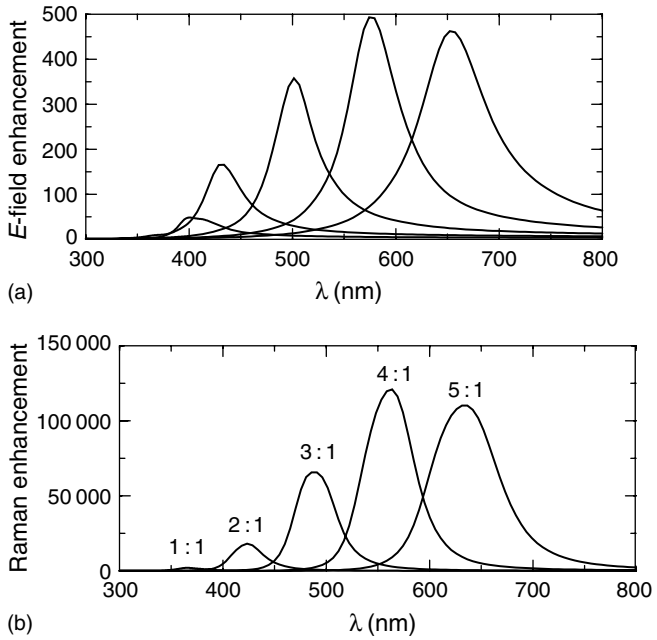

Figure 1. (a) Field enhancement R for Ag versus photon wavelength λ for spheroids having $b = 25\,\text{nm}$. The ratios of major to minor axis are: 1 : 1, 2 : 1, 3 : 1, 4 : 1 and 5 : 1. (b) Raman enhancement for $\Delta\omega = 1500\,\text{cm}^{-1}$ versus λ. Dielectric constants are from Palik.[62]

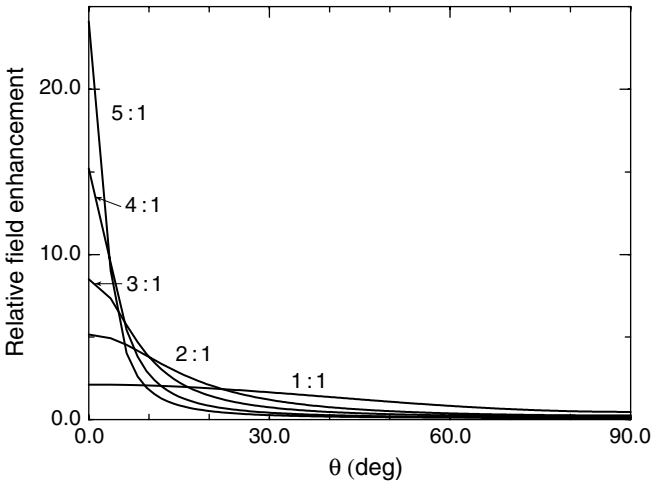

Figure 2. Ratio of local to average enhancement R for the same Ag spheroids as in Figure 1 as a function of the polar angle θ. (The graph is symmetric with respect to $\theta = 90^\circ$ so only $\theta \leq 90^\circ$ is plotted.)

each spheroid. The quantity plotted is the ratio of the local field enhancement factor to the average enhancement factor for the same spheroid, i.e. $R(\omega, \eta)/R(\omega)$ from equations (9) and (15). Note that the sphere result ($b/a = 1.0$) reproduces the θ dependence described earlier. For highly prolate spheroids, i.e. $b/a = 4 : 1$ and $5 : 1$, the field enhancement at the tip is very large, 10–25 times larger than the average enhancement. This means that the peak Raman

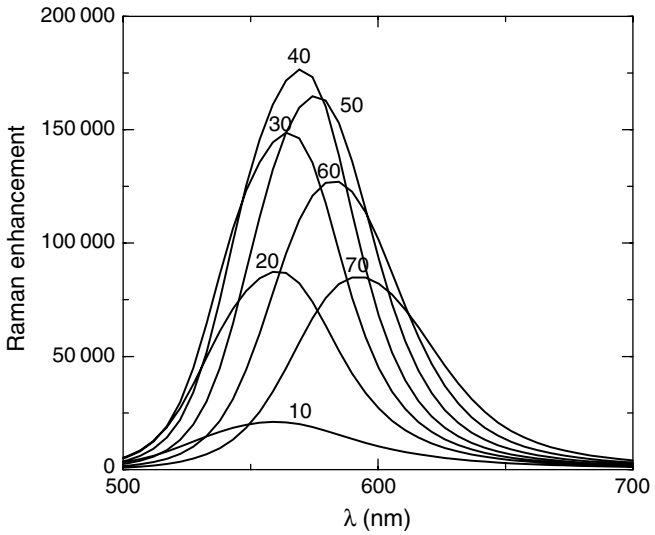

Figure 3. Raman enhancement R for a 4 : 1 Ag spheroid (using the same parameters as in Figure 1) as a function λ for values of the semimajor axis parameter b ranging from 10 to 70 nm.

enhancement should be 10^2–10^3 larger than the average Raman enhancement, so if the average enhancement is 10^6, the peak enhancement would be 10^9.

The results in Figure 1 refer to a fixed semimajor axis of 25 nm. Figure 3 shows the Raman enhancements that are obtained if this axis size is allowed to vary in the range 10–70 nm for 4 : 1 spheroids. This figure shows that the enhancement rises to a peak at $b = 40\,\text{nm}$, with the peak enhancement being close to double what it was for $b = 25\,\text{nm}$. This optimum arises from the competing effects of the electrodynamics corrections (which favor smaller objects) and the size-dependent dielectric constants (which favor larger objects). Note also that larger spheroids produce red-shifted plasmon resonances due to electrodynamic effects.

Figure 4 shows the peak Raman enhancement factor $\mathscr{E}_\text{R}$ as a function of photon wavelength. In this figure the enhancement has been optimized with respect to size and shape for each wavelength. Several metals have been considered, including the noble metals (for which SERS has been well characterized), the alkali metals, Al and In (for which there have been a few reports), and other metals (Ga, Zn, Cd) for which there are no clear-cut SERS observations. The dielectric constants in this case are from Hagemann *et al.*[63] For Ag, we find an enhancement factor close to 10^5 for $\lambda = 730\,\text{nm}$, which drops slowly with decreasing λ. The corresponding results for Ag using the Palik dielectric constants (derived from Figure 3) show peak enhancement factors that are about a factor of 2 larger, and which peak at about 600 nm. The Cu and Au results in Figure 3 show large enhancements ($>10^4$) for wavelengths longer than 700 nm, then a dramatic drop-off at

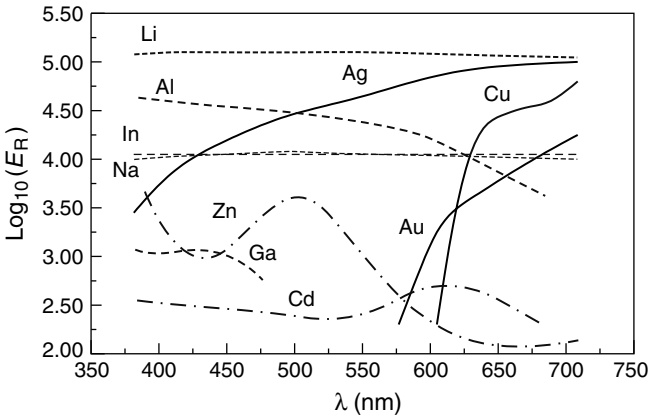

Figure 4. Fully optimized Raman enhancement (optimized with respect to size and shape) versus λ. Adapted from Zeman and Schatz,[25] Figure 22. The dielectric constants are from Hagemann *et al*.[63]

shorter wavelengths corresponding to the onset of interband excitation, which greatly increases the imaginary part of the dielectric constant.

Although Figure 4 serves as a useful guide in quantifying the EM for a variety of metals, the detailed comparison with experiment must be done with some caution as the experiments have almost always been done with an unknown or poorly characterized distribution of roughness features. One exception refers to the well-known experiments by Liao and co-workers[71] on microlithographically prepared "posts". The wavelength dependence of the SERS intensities for both Ag and Au posts has been successfully modeled[71] using a spheroid electromagnetic model that is almost identical to that described above. (The dynamic depolarization term was not included.) In this modeling, the shape of the spheroid was adjusted so that the plasmon resonance wavelength matched experiment, a procedure that is necessary because the shape and size of the particle, as well as the underlying substrate, cannot be controlled accurately enough to develop a parameter-free comparison between theory and experiment. Recent studies using lithographic methods with colloidal crystal masks have produced triangular-shaped particles whose extinction spectra,[72] as well as substrate and solvent effects,[73] may be explained quantitatively using parameter-free electrodynamics calculations. Although it is not yet clear how well EM theory will do in describing SERS on these particles (Yang *et al*.[26] describe an initial attempt in this direction), this at least provides a benchmark for EM estimates.

One issue concerning Figure 4 that deserves further note is the comparison of absolute enhancement factors with experiment. For Ag at 515 nm, Figure 3 indicates an optimized enhancement factor of 4×10^4 while experimental enhancements are typically $(1-3) \times 10^6$ for electrochemical experiments,[2,3] and about 10^5 for ultrahigh vacuum measurements.[71] Although larger enhancements (10^5) are obtained from the Palik dielectric constants, there is still a gap between electromagnetic theory and experiment, presumably due to the chemical enhancement mechanism. For Cu and Au there is a similar gap between theory and experiment, although the drop in intensity at 600 nm in Figure 4 matches observations accurately.[74] Experimental information concerning the magnitudes and frequency dependence of the enhancements for the alkalis Al and In is not extensive. Although the available results are roughly consistent with Figure 4, a chemical enhancement factor may also be present.

One experiment that provides an important test for the electromagnetic model is the observation of SERS by Jennings *et al*.[75] at an excitation wavelength of 1.06 μ (1.17 eV) for molecules adsorbed on Au metal island films and CaF_2 roughened Au films. The estimated enhancement factor was 50–100. This extends the range of SERS observations to much longer wavelengths than in previous measurements (for which $\lambda < 650$ nm was the typical limit). Qualitatively one expects a reduction in enhancement compared with the visible, since only needle-shaped or pancake-shaped particles have plasmon resonances in the near-infrared (NIR), and most of the molecules on these needles or pancakes, are located away from the tips where enhancements are relatively small (as in Figure 2). However, there are no quantitative comparisons between theory and experiment for this case.

The determination of adsorbate geometry and orientation is one of the most important features of the chemical information content of SERS. An early example demonstrating that relative intensity pattern in SERS was sensitive to adsorbate orientation was given by Allen *et al*.[76] for the case of 2-, 3- and 4-cyanopyridine. Moskovits and Suh[77] have given a general discussion of this, and Creighton[78] has provided an extensive review of surface selection rules for SERS. There are many applications of this sort in the SERS literature for a large number of different molecules, including phthalizine, substituted benzenes and carboxylic acids by Moskovits and co-workers,[77,79,80] monosubstituted benzenes by Weaver and co-workers,[81] and a variety of alkanethiols by Pemberton *et al*.[82] The conclusions regarding adsorbate geometry and orientation in these studies, by and large, make good "chemical" sense.

In spite of these successes, a significant number of papers continue to be published in which the residual uncertainty over the relative contributions of the electromagnetic and chemical enhancement mechanisms in SERS is interpreted by the authors to preclude the capability of determining adsorbate geometry and orientation. This is reflected in the wider surface science community by a

certain reluctance or nervousness to embrace such conclusions from SERS studies. Consequently, a few remarks concerning the surface selection rules of SERS are appropriate here.

Provided that one uses a SERS-active surface for which the EM dominates, one can indeed use the relative intensity pattern to determine adsorbate geometry and orientation. To draw such conclusions in a quantitative manner, one needs at make an estimate of the relative magnitudes of the electric fields parallel and perpendicular to the surface, something that is easily extracted from the spheroid model. In addition, one needs at least qualitative information about the polarizability derivative tensor of the molecule and modes being studied. This information is now readily available from ab initio quantum chemistry calculations. Thus it is possible to predict the relative SERS intensity pattern as a function of adsorbate geometry and orientation. A detailed example of this for the case of *trans*-1,2(4-pyridyl)ethylene (BPE) adsorbed onto silver film over nanosphere electrodes has been published by Yang *et al*.[83] For usage in a more qualitative sense, one can simply note that since electric field components are largest perpendicular to the surface, modes involving large changes in the perpendicular polarizability are most strongly enhanced.

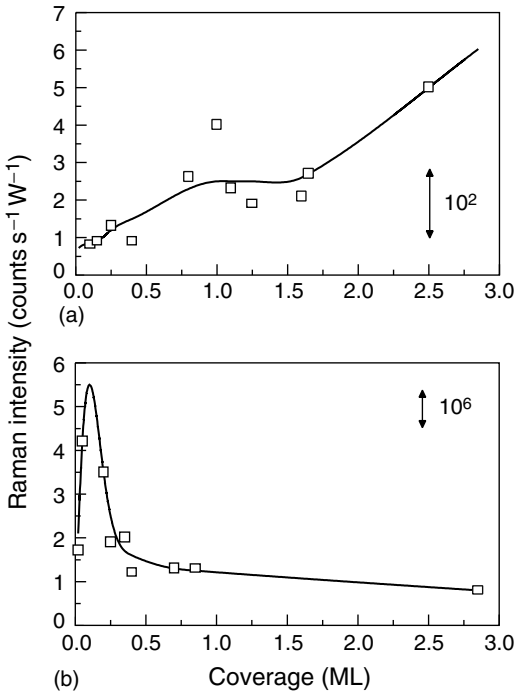

Figure 5. Coverage dependence of the 683-cm^{-1} line of CoPc: (a) CoPc on a thick Cr (unenhancing substrate) using laser power of 300 mW; (b) CoPc on a roughened Ag substrate using 10 nW power.

3 EXTENSIONS OF THE ELECTROMAGNETIC MODEL

3.1 Effect of adsorbed layers on intensities

The electromagnetic model as developed to this point considers a metal particle of dielectric constant ε_{i} embedded in a homogeneous medium of dielectric constant ε_{o}. Several experiments done since 1984 have demonstrated that an adsorbed layer can significantly alter enhancements (changing both magnitude and frequency dependence) even when present in relatively low coverages ($\sim$0.1 monolayers).

Both theory and experiments concerning the effect of adsorbed layers on SERS have been presented by Murray and Bodoff,[84,85] Murray,[37] and Waseleski *et al*.[36] and a related treatment of surface-enhanced resonance Raman scattering (SERRS) has been given by Zeman *et al*.[35] In the Murray and Bodoff experiments, the SERS intensity for CN^- adsorbed onto silver island films was found to vary nonlinearly with coverage, with a peak at about 0.25 monolayers, and falling intensities at higher coverages. In the Zeman *et al*. experiments, a similar dependence on coverage was found for SERRS of cobalt phthalocyanine (CoPc) on roughened silver films, with a peak at 0.07 monolayer. Figure 5 shows the latter results, contrasting the SERRS intensities with the corresponding spectra on an unenhancing substrate.

The coverage dependence of SERS and SERRS can be explained using a simple extension of the spheroid model presented previously in which the spheroid is assumed to be coated with a layer whose dielectric constant is denoted ε_l. If the layer is assumed to be defined as the region between two confocal spheroidal surfaces, then the solution of LaPlace's equation is very similar to that in equation (9), but with $R(\omega)$ multiplied by an additional layer-dependent factor. Surface coverage in this model may either be described by varying the layer thickness, or by using an effective medium approximation to express the layer dielectric constant ε_l in terms of the adsorbate and solvent dielectric constants.

An alternative theory of coverage effects in SERS and SERRS has been developed by Murray and Bodoff[84,85] and by Zeman *et al*.[35] based on the explicit treatment of the interaction of adsorbed molecules with the applied field, with the metal particle, and with each other. In this theory, the molecules and the metal particle are replaced by polarizable dipoles $\boldsymbol{\mu}_i$. The magnitudes of these dipoles are determined by solving the usual coupled dipole (CD) equations:

$$\boldsymbol{\mu}_i = \alpha_i \left(\mathbf{E}_{\mathrm{o}} + \sum_{j \neq i} M_{ij} \boldsymbol{\mu}_j \right) \tag{26}$$

where $\mathbf{E}_{\mathrm{o}}$ is the applied field, α_i is the polarizability of the ith dipole, and M_{ij} is the dipole interaction between the ith

and jth dipoles:

$$M_{ij}\boldsymbol{\mu}_j = \left[k^2(\mathbf{r}_{ij}\times\boldsymbol{\mu}_j)\times\mathbf{r}_{ij}\frac{e^{i\mathbf{k}\cdot\mathbf{r}_{ij}}}{r_{ij}^3}\right] + \left\{[3\mathbf{r}_{ij}(\mathbf{r}_{ij}\cdot\boldsymbol{\mu}_j) - r_{ij}^2\boldsymbol{\mu}_j]\left(\frac{1}{r_{ij}^5} - \frac{ik}{r_{ij}^4}\right)e^{i\mathbf{k}\cdot\mathbf{r}_{ij}}\right\} \quad (27)$$

For molecules on a flat surface[84,85] only dipole coupling between molecules is included, and equation (26) may be solved analytically (in the static, $k \to 0$, limit) as long as the molecules occupy sites on a square lattice. For molecules on a metal particle, equation (26) must be solved numerically. Usually the interactions between dipoles are too strong to allow for its solution by iteration, but as long as the number of molecules is not too large, equation (26) may be solved by direct inversion for assumed locations of the molecules. By averaging over a sufficient number of molecular locations that are consistent with the desired surface coverage, the realistic simulation of experiments is possible.

Figure 6 shows the CD predictions for SERRS intensity versus coverage for CoPc on silver. Several choices of spheroid shape are included, as are two choices of Stokes shift. The figure shows that the more prolate the metal particle, the lower the coverage where intensity peaks. At the observation wavelength (647.1 nm), Figure 1 indicates that 4 : 1 and 5 : 1 spheroids should be dominant. Figure 6 then indicates that intensities should peak at about 0.1 monolayer, which is consistent with results in Figure 5.

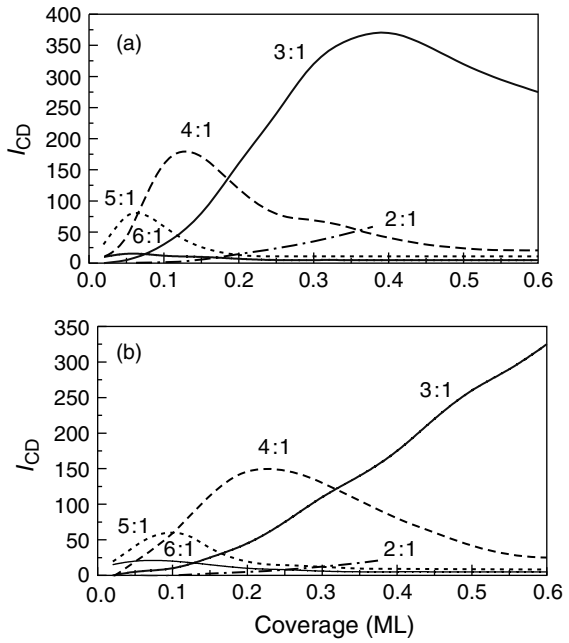

Figure 6. CD model Raman intensities I_{CD} for Ag spheroids having $b = 12$ nm versus coverage for $\hbar\omega = 1.916$ eV: (a) $\Delta\omega = 683\,\mathrm{cm}^{-1}$; (b) $\Delta\omega = 1544\,\mathrm{cm}^{-1}$.

Calculations using the layered spheroid model for the same parameters as in Figure 5 give similar results, indicating that approximations involved in both models are not important to the final results. The layered model has been used by Murray[37] to describe SERS from particles coated with an overlayer upon which molecules are adsorbed. In this case the molecules experience the field induced at the outer surface of the coating. Detailed studies of silver particles coated with a layer of gold, nickel or insulators were carried out,[37] and these demonstrated that substantial damping and shifting of the plasmon resonance can be induced by the layer.

Although these results all seem very encouraging, we should point out that layer and dipole models of solvent effects on the extinction spectra of silver nanoparticles often seriously overestimate the shift of the plasmon wavelength as solvent dielectric constant is increased.[73] This suggests that chemical interactions between nanoparticle and solvent could cause the electromagnetic environment near the surface to be significantly different from the simple model. This indicates that caution should be applied in interpreting the significance of the results in Figures 5 and 6.

3.2 Nonlinear surface optical processes

As mentioned in the introduction, the electromagnetic model can be used with no additional computational effort to predict enhancement factors for surface-enhanced nonlinear spectroscopies, including SESHG and SEHRS. This assumes that the nonlinearity is determined by the field or field gradient at the interface, which is a reasonable but not completely correct assumption. At present, the quality of theory/experiment comparisons is not high enough to quantify the error involved, but some theoretical estimates have been provided for SESHG.[38–41]

The relevant enhancement factors (analogous to equation 8) are given by

$$\mathrm{SESHG}(\omega' = 2\omega)\colon \mathscr{E}_{\mathrm{SHG}} = R(2\omega)R^2(\omega) \quad (28)$$

$$\mathrm{SEHRS}(\omega' = 2\omega - \Delta)\colon \mathscr{E}_{\mathrm{HRS}} = R(2\omega - \Delta)R^2(\omega) \quad (29)$$

where R denotes the field enhancement factor from equation (9).

Now let us consider specific examples in which $\mathscr{E}_{\mathrm{SHG}}$ has been compared with experiment. We restrict our discussion to experiments where isolated particle models can be used. The next section provides discussion of other types of surfaces like gratings. Table 1 presents a comparison of the SHG enhancement factors for several metals (Ag, Au, Cu, Li, Na, Al, Ga and In) at $\hbar\omega = 1.17$ eV. The two theoretical calculations refer to averages over spheroid sizes and shapes

Table 1. SHG enhancement factors.

Metal	$\mathscr{E}_{SHG}$	$\mathscr{E}_{SHG}$ (normalized to Ag)		
	Theory[a]	Theory[a]	Theory[b]	Expt[b]
Ag	1.5×10^6	1	1	1
Au	8.4×10^4	0.06	0.10	0.008
Cu	8.3×10^4	0.06	0.10	0.01
Li	4.6×10^4	0.03	–	–
Na	3.3×10^5	0.22	0.16	0.36
Al	3.6×10^5	0.24	0.40	4.6
Ga	9.5×10^6	6.3	4.0	27.0
In	1.2×10^4	0.01	0.04	0.004

[a]Taken from Zeman and Schatz.[25]
[b]Taken from Boyd *et al*.[87]

such that the volume is in the range $10^{-5}\lambda^3$ to $10^{-4}\lambda^3$. The averages used in the two studies[25,86,87] were not the same, but the resulting enhancements are similar. The results from Zeman and Schatz[25] are given both as absolute and relative enhancements (normalized to Ag), while the other two enhancements are only available as relative enhancements.

The comparison between theory and experiment is generally quite good for the relative enhancements, with Ga showing the largest value for each column in Table 1. Only the result for Al is in serious error, otherwise the variation with metal is correct. The absolute enhancement factors in Table 1 are generally larger than the SERS factors in Figure 4, but not by much. Ga, however, shows much larger SHG than SERS.

Figure 7 presents the calculated SHG enhancement factor for Pt spheroids[42] over a range of photon energies. Although Pt does not show significant electromagnetic enhancement effects in the visible, at $\lambda = 1060$ nm enhancements of a few hundred are possible. This result is consistent with the observation[42] of SESHG from rippled Pt microstructures where the ripple size is comparable to that used in the electromagnetic modeling. This demonstrates the potential broad applicability of SESHG, as many metals show dielectric behavior similar to Pt (i.e. small SHG enhancements in the visible, but significant enhancements in the NIR). In fact, for Pt, Figure 7 indicates that SESHG enhancements are even larger for $\lambda > 2000$ nm.

There has been relatively little theoretical work done on SEHRS, but Golab *et al*.[88] and Yang and Schatz[89] have provided important results concerning the SEHRS enhancement factor for pyridine and BPE adsorbed onto roughened silver. This enhancement factor is difficult to measure directly because when SEHRS is observable, the corresponding bulk hyper-Raman scattering measurement requires extreme laser powers that are difficult to quantify. (See, however, the work of Johnson and co-workers[90,91] for one attempted measurement.) An indirect method for

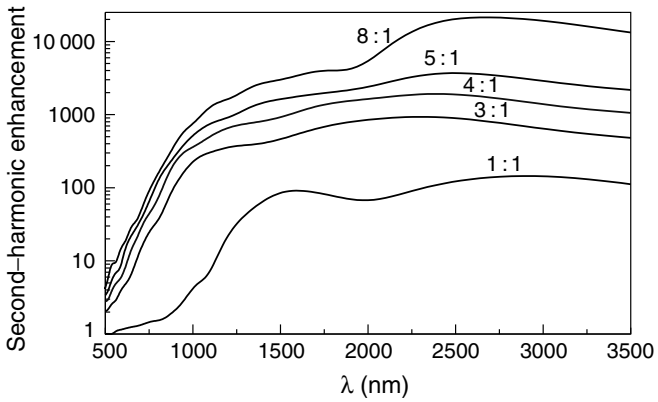

Figure 7. Predicted SESHG enhancement factor S as a function of input photon wavelength λ for a Pt spheroid having $b = 200$ nm and $b/a = 8:1$, $5:1$, $4:1$, $3:1$ and $1:1$.

determining SEHRS enhancements involves determining the terms in the expression[88]

$$\frac{I_{HR}^{srf}}{I_{HR}^{bulk}} = \left(\frac{I_{R}^{srf}}{I_{R}^{bulk}}\right)\left(\frac{I_{HR}^{srf}}{I_{R}^{srf}}\right)\left(\frac{I_{HR}^{bulk}}{I_{R}^{bulk}}\right)^{-1} \tag{30}$$

The first term on the right-hand side is the well-known 10^6 SERS enhancement factor. The second term is the ratio of hyper-Raman to Raman intensities on the surface, which is a quantity that can be obtained straightforwardly from experiment. The third term is the corresponding bulk ratio. This is hard to obtain from experiment (although estimates do exist),[88] but can be obtained from molecular orbital calculations as it involves isolated molecule properties. The best estimate of this ratio is from Yang and Schatz,[89] who used Hartree–Fock methods with a basis set that includes polarization and diffuse functions. To calibrate their results, they calculated Raman spectra from benzene, and were able to match high-quality gas-phase measurements. In addition, their bulk hyper-Raman spectra were consistent with available measurements.

The SEHRS enhancement obtained by Yang and Schatz[89] was in the range 10^{11}–10^{12}. This is much larger than is predicted by the electromagnetic model (for which the SHG enhancement factor for Ag in Table 1 provides a realistic estimate). The likely explanation for the discrepancy is that chemical enhancement mechanisms are much more important for SEHRS than they are for SERS. This is in accord with the strong sensitivity that the molecular hyperpolarizability shows to the presence of excited states that have a significant change in dipole moment relative to the ground state. Such states are not important for gas-phase pyridine, but they are easily produced when molecules are adsorbed on surfaces via charge transfer between the molecule and surface.

4 ELECTROMAGNETIC MECHANISM FOR MANY COUPLED PARTICLES AND FOR GRATINGS

The theoretical development to this point has considered only isolated particles. In most cases, experiments involve more complex surfaces so it is important to develop electrodynamics theory for more general applications. This section is concerned with the problem of modeling many coupled particles, or extended structures such as gratings and randomly roughened continuous surfaces. As with several earlier parts of this review, substantial work on this topic was carried out before 1985, and has been reviewed already. Our discussion of this work will therefore be representative rather than exhaustive.

The simplest coupled particle system is just two coupled spheres. LaPlace's equation was solved for this problem by Aravind *et al.*[92] and the results were used to study the field enhancement in the region between the spheres. This enhancement can become very large under certain circumstances.

The next more complicated problem involves treating many coupled particles, either in a regular array, as was done elsewhere[93–96] for spheres, or in a random array, as was done elsewhere[31,32] for spheroids. In either case, densely packed arrays exhibit substantially different plasmon resonance features that are associated with isolated particles, including multiple resonances that can be either red- or blue-shifted relative to the single particle resonances.[32,93,94]

There has been substantial recent work concerned with particle coupling effects in the context of extinction spectra that goes beyond the simple dipole coupling theories.[95,96] This work shows that the dipole approximation is adequate for small particles (10 nm) provided that the particles are separated by a particle radius or more.

Gratings are another type of extended surface that has received considerable attention in applications of the EM. There have been several theoretical studies of SERS on gratings (see Garcia *et al.*[97] and references therein), and the calculated maximum enhancements are similar in magnitude to what has been calculated for spheroids that have comparable size features to the grating corrugation. The maximum SERS enhancement occurs for incident angles and grating structures where reflectivity minimizes, as that leads to the maximum conversion of incident photon energy to plasmon energy.

Gratings and other types of surface roughness have also been considered in studies of SESHG. The literature on this topic is quite extensive, including several electrodynamics studies.[98–101] There has also been extensive work on calculating nonlinear susceptibilities (see Sipe *et al.*[102] and Schaich and Mendoza[103] and references therein.) For Ag gratings, the largest measured enhancement factor found so far is 7000.[104] This result is in good agreement with theoretical predictions. An optimum groove depth is also found that is similar to that found for SERS.[105] Recently it has been demonstrated both theoretically and experimentally that SESHG on gratings can be selectively enhanced by using a grating that has two spatial frequencies, one that couples the incident light to plasmon excitation at the fundamental frequency, and the other that couples the second-harmonic plasmon to the emitted photon.[106,107]

5 CONCLUSIONS AND FURTHER WORK

This review has dealt mostly with features of the electromagnetic model that correlates well with experiment, but it is important to mention features where the relation between theory and experiment merits further work. We will leave out of this discussion problems such as the SEHRS enhancement factor where it appears that the primary discrepancy between theory and experiment is associated with chemical contributions to the enhancement.

Perhaps the key weakness in the comparison between electromagnetic theory calculations and SES measurements lies in the mismatch between the surface modeled and that measured. Most measurements refer to randomly roughened surfaces that have important features like pores and cracks that are rarely included in calculations. Only a few experiments on well-characterized surfaces (periodic arrays of posts, gratings) have been performed. Most calculations have modeled isolated particles or perfect gratings, with little attention given to experimental reality. Because of this, the comparison between theory and experiment is still very imprecise. This makes it difficult to explain why two rough surfaces prepared with slightly different roughening procedures may show orders of magnitude enhancement differences (as sometimes happens). Also, it is difficult to quantify the fraction of molecules that experience substantial SERS enhancements.

A second problem that is connected closely to the first refers to the complexity of accurate solutions of Maxwell's equations for arbitrarily irregular surfaces that have roughness comparable in size to the wavelength of light. LaPlace's equation has often been used, but it can be inaccurate. Numerical solutions are possible but may not be worth the significant computational expense for poorly characterized surfaces. A better solution would be to have more experiments done on structurally simple surfaces.

A third problem is that dielectric constants are not always available at frequencies where they are needed. Even for

Ag, Au, and Cu, where dielectric constants are generally available, there are significant differences between results generated with different literature values.[64]

Finally, it should be noted that there is a significant need for experimental studies in which more than one SES measurement is done on the same surface. The comparison of SERS and SESHG would be especially interesting in testing the EM, as competing (chemical) mechanisms influence SERS but not SESHG. A grand challenge in this area would be to measure the extinction and Rayleigh scattering spectrum, along with the SERS, SESHG and SEHRS excitation profiles for the same adsorbate on a well-characterized nanofabricated surface.

ACKNOWLEDGMENTS

We would like to acknowledge several present and former members of the Schatz and Van Duyne groups who have contributed to the theory/experiment collaboration that is described in this review. This research was supported by ARO Grant DAAG559710133, and by the MRSEC program of the NSF (Grant DMR-0076097) at the Materials Research Center of Northwestern University.

ABBREVIATIONS AND ACRONYMS

BPE	*trans*-1,2(4-pyridyl)Ethylene
CD	Coupled Dipole
CoPc	Cobalt Phthalocyanine
EM	Electromagnetic Mechanism
SEHRS	Surface-enhanced Hyper-Raman Spectroscopy
SES	Surface-enhanced Spectroscopy
SESHG	Surface-enhanced Second-harmonic Generation
SPIRS	Surface Phonon-induced Raman Scattering

REFERENCES

1. M. Fleischman, P.J. Hendra and A.J. McQuillan, *Chem. Phys. Lett.*, **26**, 163 (1974).
2. D.L. Jeanmaire and R.P. Van Duyne, *J. Electroanal. Chem.*, **84**, 1 (1977).
3. M.G. Albrecht and J.A. Crieghton, *J. Amer. Chem. Soc.*, **99**, 5215 (1977).
4. M. Moskovits, *Rev. Mod. Phys.*, **57**, 783 (1985).
5. A. Otto, *Top. Appl. Phys.*, **54**, 289 (1984).
6. H. Metiu, in "Surface Enhanced Raman Scattering", eds T.E. Furtak and R.K. Chang, Plenum, New York (1981).
7. H. Metiu and P. Das, *Annu. Rev. Phys. Chem.*, **35**, 507 (1984).
8. M. Kerker, *Acct. Chem. Res.*, **17**, 271 (1984).
9. M. Kerker (ed.), 'Selected Papers on Surface-enhanced Raman Scattering', SPIE Optical Engineering Press, Bellingham, WA (1990).
10. G.C. Schatz, *Acct. Chem. Res.*, **17**, 370 (1984).
11. H. Metiu, *Prog. Surf. Sci.*, **17**, 153 (1984).
12. S. Efrima, 'Surface-enhanced Raman Scattering (SERS)', in "Modern Aspects in Electrochemistry", eds J.O'M. Bockris, R. White and B.E. Conway, Plenum, New York, 253–369, Vol. 16 (1986).
13. A. Campion and P. Kambhampati, *Chem. Soc. Rev.*, **27**, 241 (1998).
14. E.J. Liang and W. Kiefer, *J. Raman Spectrosc.*, **27**, 879 (1996).
15. R.G. Greenler and T.L. Schlager, *Spectrochim. Acta*, **A29**, 193 (1973).
16. M. Moskovits, *J. Chem. Phys.*, **69**, 4159 (1978).
17. S.L. McCall, P.M. Platzman and P.A. Wolff, *Phys. Lett.*, **77A**, 381 (1980).
18. D.-S. Wang, H. Chew and M. Kerker, *Appl. Opt.*, **19**, 2256 (1980).
19. D.-S. Wang and M. Kerker, *Phys. Rev.*, **B24**, 1777 (1981).
20. M. Kerker, D.-S. Wang and H. Chew, *Appl. Opt.*, **19**, 4159 (1980).
21. M. Kerker, *J. Coll. Interface Sci.*, **118**, 417 (1987).
22. J. Gersten and A. Nitzan, *J. Chem. Phys.*, **73**, 3023 (1980).
23. F.J. Adrian, *Chem. Phys. Lett.*, **78**, 45 (1981).
24. P.W. Barber, R.K. Chang and H. Massoudi, *Phys. Rev.*, **B27**, 7251 (1983).
25. E.J. Zeman and G.C. Schatz, *J. Phys. Chem.*, **91**, 634 (1987).
26. W.-H. Yang, G.C. Schatz and R.P. Van Duyne, *J. Chem. Phys.*, **103**, 869 (1995).
27. J.P. Kottmann, O.J.F. Martin, D.R. Smith and S. Schultz, *Optics Express*, **6**, 213 (2000).
28. M. Arnold, P. Bussemer, K. Hehl, H. Brabhorn and A. Otto, *J. Mod. Opt.*, **39**, 2329 (1992).
29. I. Baltog, N. Primeau, R. Reinisch and J.L. Coutaz, *Appl. Phys. Lett.*, **66**, 1187 (1995).
30. N. Garcia, *Opt. Commun.*, **45**, 307 (1983).
31. U. Laor and G.C. Schatz, *J. Chem. Phys.*, **76**, 2888 (1982).
32. U. Laor and G.C. Schatz, *Chem. Phys. Lett.*, **82**, 566 (1981).
33. J.A. Sanchez-Gil and J.V. Garcia-Ramos, *J. Chem. Phys.*, **108**, 317 (1998).
34. W.A. Kraus and G.C. Schatz, *J. Chem. Phys.*, **79**, 6130 (1983).
35. E.J. Zeman, K.T. Carron, G.C. Schatz and R.P. Van Duyne, *J. Chem. Phys.*, **87**, 4189 (1987).
36. S.A. Waseleski, S. Zou and M.J. Weaver, *Appl. Spectrosc.*, **54**, 761 (2000).
37. C.A. Murray, *J. Opt. Soc.*, **B2**, 1330 (1985).
38. G.S. Agarwal and S.S. Jha, *Solid State Commun.*, **41**, 499 (1982).

39. X.M. Hua and J.I. Gersten, *Phys. Rev. B*, **33**, 3756 (1986).
40. D. Ostling, P. Stampfli and K.H. Bennemann, *Z. Phys. D*, **28**, 169 (1993).
41. J.I. Dadap, J. Shan, K.B. Eisenthal and T.F. Heinz, *Phys. Rev. Lett.*, **83**, 4045 (1999).
42. K.L. Haller, L.A. Bumm, R.I. Altkorn, E.J. Zeman, G.C. Schatz and R.P. Van Duyne, *J. Chem. Phys.*, **90**, 1237 (1989).
43. A. Otto, *J. Raman Spectrosc.*, **22**, 743 (1991).
44. A. Otto, *Surf. Sci.*, **75**, L3926 (1978).
45. P.K.K. Pandey and G.C. Schatz, *J. Chem. Phys.*, **80**, 2959 (1984).
46. T. Maniv and H. Metiu, *Chem. Phys. Lett.*, **79**, 79 (1981).
47. S.L. McCall and P.M. Platzman, *Phys. Rev. B*, **22**, 1660 (1980).
48. S.S. Jha, J.R. Kirtley and J.C. Tsang, *Phys. Rev. B*, **22**, 3973 (1980).
49. S. Mamiche-Afara and M.J. Dignam, *J. Chem. Phys.*, **90**, 3861 (1989).
50. T. Maniv and H. Metiu, *Surf. Sci.*, **101**, 399 (1980).
51. P.J. Feibelman, *Phys. Rev. B*, **22**, 3654 (1980).
52. F.J. Adrian, *J. Chem. Phys.*, **77**, 5302 (1982).
53. C.R. Bohren and D.F. Huffman, 'Absorption and Scattering of Light by Small Particles', John Wiley & Sons, New York (1983).
54. M. Meier and A. Wokaun, *Opt. Lett.*, **8**, 581 (1983).
55. E. Zeman and G.C. Schatz, in "Dynamics on Surfaces, Proceedings of the 17th Jerusalem Symposium", eds B. Pullman, J. Jortner, B. Gerber and A. Nitzan, Reidel, Dordrecht, 413–424 (1984).
56. U. Kreibig and C.v. Fragstein, *Z. Phys.*, **224**, 307 (1969).
57. J. Euler, *Z. Phys.*, **137**, 318 (1954).
58. L. Genzel, T.R. Martin and U. Kreibig *Z. Phys.*, **21**, 339 (1975).
59. M. Xu and M.J. Dignam, *J. Chem. Phys.*, **96**, 3370 (1992).
60. W.A. Kraus and G.C. Schatz, *Chem. Phys. Lett.*, **99**, 353 (1983).
61. A. Liebsch and W.L. Schaich, *Phys. Rev. B: Condens. Matter*, **52**, 14219 (1995).
62. D.W. Lynch and W.R. Hunter, 'Comments on the Optical Constants of Metals and an Introduction to the Data for Several Metals', in "Handbook of Optical Constants of Solids", ed E.D. Palik, Academic Press, New York, 350–356 (1985).
63. H.J. Hagemann, W. Gudat and C. Kunz, DESY Report No. SR-74/7, May (1984).
64. M. Kerker, *J. Opt. Soc. B*, **2**, 1327 (1985).
65. S. Nie and S.R. Emory, *Science*, **275**, 1102 (1997).
66. K. Kneipp, H. Kneipp, G. Deinum, I. Itzkan, R.R. Dasari and M.S. Feld, *Appl. Spectrosc.*, **52**, 175 (1998).
67. A.M. Michaels, M. Nirmal and L.E. Brus, *J. Am. Chem. Soc.*, **121**, 9932 (1999).
68. K. Kneipp, H. Kneipp, I. Itzkan, R.R. Dasari and M.S. Feld, *Chem. Rev.*, **99**, 2957 (1999).
69. H. Xu, E.J. Bjerneld, M. Käll and L. Börjesson, *Phys. Rev. Lett.*, **83**, 4357 (1999).
70. T. Jensen, L. Kelly, A. Lazarides and G.C. Schatz, *J. Cluster Sci.*, **10**, 295 (1999).
71. P.F. Liao and M.B. Stern, *Opt. Lett.*, **7**, 483 (1982).
72. T.R. Jensen, G.C. Schatz and R.P. Van Duyne, *J. Phys. Chem. B*, **103**, 2394 (1999).
73. T.R. Jensen, M.L. Duval, K.L. Kelly, A. Lazarides, G.C. Schatz and R.P. Van Duyne, *J. Phys. Chem.*, **103**, 9846 (1999).
74. C.S. Allen, G.C. Schatz and R.P. Van Duyne, *Chem. Phys. Lett.*, **75**, 201 (1980).
75. C.A. Jennings, G.J. Kovacs and R. Aroca, *J. Phys. Chem.*, **96**, 1340 (1992).
76. C.S. Allen and R.P. Van Duyne, *Chem. Phys. Lett.*, **63**, 455 (1979).
77. M. Moskovits and J.S. Suh, *J. Phys. Chem.*, **88**, 5526 (1984).
78. J.A. Creighton, in "Spectroscopy of Surfaces", eds R.J.H. Clark and R.E. Hesters, John Wiley & Sons, New York, 37–89, Vol. 16 (1988).
79. M. Moskovits and J.S. Suh, *J. Phys. Chem.*, **88**, 1293 (1984).
80. M. Moskovits, D.P. DiLella and K.J. Maynard, *Langmuir*, **4**, 67 (1988).
81. X. Gao, J.P. Davies and M.J. Weaver, *J. Phys. Chem.*, **94**, 6858 (1990).
82. J.E. Pemberton, M.A. Bryant, R.L. Sobocinski and S.L. Joa, *J. Phys. Chem.*, **96**, 3776 (1992).
83. W.H. Yang, J.C. Hulteen, G.C. Schatz and R.P. Van Duyne, *J. Chem. Phys.*, **104**, 4313 (1996).
84. C.A. Murray and S. Bodoff, *Phys. Rev. Lett.*, **52**, 2273 (1984).
85. C.A. Murray and S. Bodoff, *Phys. Rev. B*, **32**, 671 (1985).
86. C.K. Chen, A.R.B. de Castro and Y.R. Shen, *Phys. Rev. Lett.*, **46**, 145 (1981).
87. G.T. Boyd, T. Rasing, J.R.R. Leite and Y.R. Shen, *Phys. Rev. B*, **30**, 519 (1984).
88. J.T. Golab, J.R. Sprague, K.T. Carron, G.C. Schatz and R.P. Van Duyne, *J. Chem. Phys.*, **88**, 7942 (1988).
89. W.H. Yang and G.C. Schatz, *J. Chem. Phys.*, **97**, 3831 (1992).
90. J.P. Nedderson, S.A. Mounter, J.M. Bostick and C.K. Johnson, *J. Chem. Phys.*, **90**, 4719 (1989).
91. C.K. Johnson and S.A. Soper, *J. Phys. Chem.*, **93**, 7281 (1989).
92. P.K. Aravind, A. Nitzan and H. Metiu, *Surf. Sci.*, **110**, 189 (1981).
93. M. Inoue and K. Ohtaka, *J. Phys. Soc. J.*, **52**, 145 (1983).
94. M. Inoue and K. Ohtaka, *J. Phys. Soc. J.*, **52**, 3853 (1983).
95. A.A. Lazarides and G.C. Schatz, *J. Phys. Chem.*, **104**, 460 (2000).
96. A.A. Lazarides and G.C. Schatz, *J. Chem. Phys.*, **112**, 2987 (2000).

97. N. Garcia, G. Diaz, J.J. Sainz and C. Ocal, *Surf. Sci.*, **143**, 342 (1984).

98. G.S. Agarwal and S.S. Jha, *Phys. Rev. B*, **26**, 482 (1982).

99. R. Reinisch and M. Neviere, *Phys. Rev. B*, **28**, 1870 (1983).

100. G.A. Farias and A.A. Maradudin, *Phys. Rev. B*, **30**, 3002 (1984).

101. R.T. Deck and R.K. Grygier, *Appl. Opt.*, **23**, 3202 (1984).

102. J.E. Sipe, V.C.Y. So, M. Fukui and G.I. Stegeman, *Phys. Rev. B*, **21**, 4389 (1980)

103. W.L. Schaich and B.S. Mendoza, *Phys. Rev. B*, **45**, 14 279 (1992).

104. J.C. Quail and H.J. Simons, *J. Opt. Soc. Am.*, **B5**, 325 (1988).

105. J.L. Coutaz, M. Neviere, E. Pic and R. Reinisch, *Phys. Rev. B*, **32**, 2227 (1985).

106. A.C.R. Pipino and G.C. Schatz, *Phys. Rev. B*, **49**, 8320 (1994).

107. A.C.R. Pipino, R.P. Van Duyne and G.C. Schatz, *Phys. Rev. B*, **53**, 4162 (1996).